Assessing load-shifting potential of large-scale vapour compression heat pumps in Carnot batteries

Robin Tassenoy[a], Michel De Paepe[b] and Steven Lecompte[c]

[a] Department of Electromechanical, Systems and Metal Engineering, Ghent University, Belgium, Robin.Tassenoy@UGent.be, CA
[b] Department of Electromechanical, Systems and Metal Engineering, Ghent University, Belgium, FlandersMake@UGent – Core lab MIRO, FlandersMake, Belgium, Department of Mechanical Engineering, University of Cape Town, South Africa, Michel.DePaepe@UGent.be
[c] Department of Electromechanical, Systems and Metal Engineering, Ghent University, Belgium, FlandersMake@UGent – Core lab MIRO, FlandersMake, Belgium, Steven.Lecompte@UGent.be

Abstract:

Due to an increasing share of renewable energy in the energy mix, large-scale, long duration energy storage systems are becoming essential to ensure secure and stable energy supply. Carnot batteries, a combination of a power-to-heat, a thermal storage and a heat-to-power system, could provide a solution. Vapor compression heat pumps can be used as the power-to-heat technology in these systems. Techno-economic studies often consider load-shifting of solar PV as the main revenue stream for Carnot batteries. While its financial benefits have been analyzed, the technical feasibility has not been studied in detail. In financial appraisals, the system operation is optimized based on quarter-hourly or hourly timescales. However, it is known solar PV fluctuates at significantly smaller timescales, even down to the timescale of seconds. It should thus be verified whether the heat pump dynamics are sufficiently fast to follow these variations. A 1.5 MWe vapour compression heat pump, suitable for integration in a Carnot battery, is modelled dynamically and a control strategy suitable for load-following is proposed. Based on test samples, it is concluded that the heat pump dynamics are indeed suitable for direct load-following of solar PV. Assuming optimized control, the power uptake closely follows the setpoint with an aggregated absolute error of only 0.66 % for solar PV. The TES delivery temperature fluctuates around its setpoint and quickly returns to this point in stable power periods, as required for Carnot battery operation.

Keywords:

Carnot battery; vapour-compression heat pump; dynamic modelling; load-following; solar PV.

1. Introduction

The share of renewables in the European power generation has increased steadily over the past years, reaching 51.2 % in 2024 [1]. This increasing trend can be attributed mainly to the increase in variable renewable energies (VRE) like wind and solar, which accounted together for 28.5 and 15 % of the European [2] and worldwide [3] electricity mix in 2024, respectively. The intermittency of VRE challenges the stability of the electrical grid. Energy storage can address these problems by power and voltage smoothing, energy management, frequency regulation, peak shaving, load leveling, seasonal storage and standby generation during a fault [4].

Carnot batteries (CB) are an emerging storage concept that might contribute to these services. The storage concept involves thee energy processes. First, electrical energy is converted into heat (or cold) using a power-to-heat system. Then, this heat (or cold) is stored in a thermal energy storage system. Finally, a heat-to-power technology is used to convert the heat back to electricity when needed. A wide range of technologies fit this definition. Dumont et al. [5] were among the first to give an overview of different possible technologies and configurations of Carnot batteries, the state-of-the-art in experimental prototypes and key performance indicators. One of the Carnot battery's subsets is pumped thermal energy storage (PTES), in which an electrically driven heat pump elevates the temperature of heat coming from a cold source and delivers this to a thermal storage system at higher temperature [6]. Vecchi et al. [7] collected and compared the theoretical

performance data of different Carnot batteries, and discussed the applications of Carnot batteries at energy system scale.

The literature reveals that PTES has been considered mainly for load-shifting and arbitraging services. In particular, local load-following of solar PV production is almost always assumed [8, 9, 10, 11]. While the financial benefits of this service have been demonstrated, the technical feasibility is not studied in detail. Techno-economic studies often use quarter hourly or even hourly timesteps. While such timesteps are useful to evaluate the financial appraisal over one or multiple years, it is known that solar PV fluctuates at significantly smaller timescales, even down to the timescale of seconds [12, 13]. Resistive heaters can modulate power flexibly. However, it should still be verified explicitly whether vapour compression heat pumps can modulate sufficiently fast to follow these variations.

This contribution presents a dynamic model of a 1.5 MWe variable-speed, vapour compression heat pump to explicitly verify whether direct load-following of solar PV is feasible for large-scale heat pumps in PTES, as is typically assumed in techno-economic studies. For this service, the electrical response of the heat pump is of interest, in contrast to traditional heat pump applications where the thermal response is studied. Although the boundary conditions of the heat pump are selected based on a PTES case study, the results obtained are generally applicable to large-scale variable-speed heat pump applications where the power response is important. This study thus also applies to the corresponding research gap within the field of industrial heat pumps.

2. Methodology

2.1. Carnot battery lay-out and heat pump boundary conditions

In literature, several lay-outs for Rankine-based PTES have been proposed. The topology assumed here is schematically represented in Figure. **1**. The complete system consists of the vapour compression heat pump of interest, two-tank liquid thermal energy storage (TES) and an organic Rankine cycle (ORC). Such a topology is commonly evaluated in techno-economic studies, making this assessment align to the state-of-the-art.

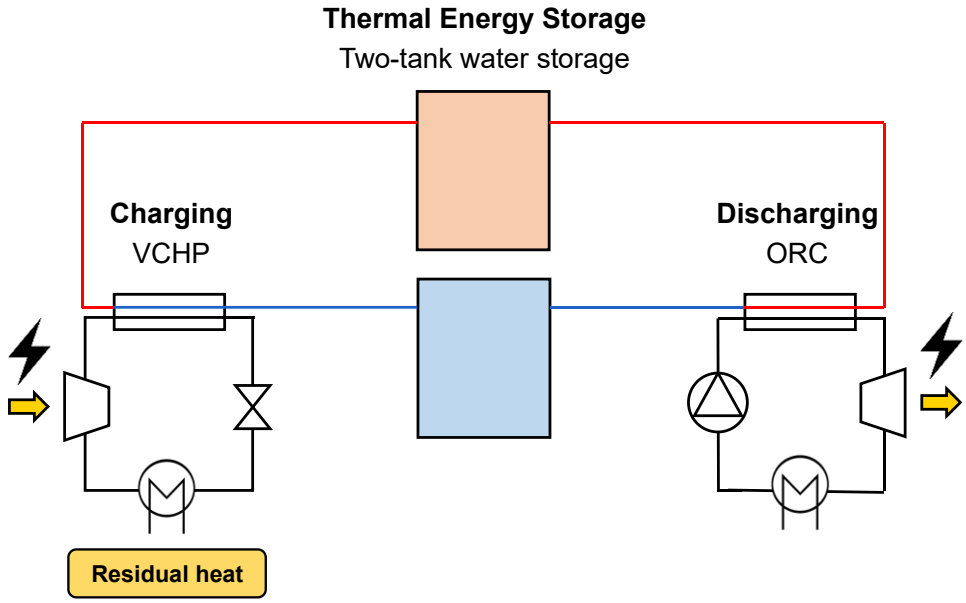

Figure. 1. *Schematic representation of a thermally integrated Rankine-based PTES.*

Rankine-based PTES typically takes advantage of a low-grade heat source to boost the electrical round-trip efficiency of the system [14]. This study assumes residual heat from a 200 m³/h waste water stream at 60 °C in a paper pulp plant, based on personal communication with a paper manufacturer. However, significant amounts of residual heat at similar temperature and power level are available in other sectors [15], making the results more applicable. The waste water stream is currently cooled down to 40 °C by a cooling tower, resulting in an available thermal heat source of 4.57 MWth.

Considering this available heat source and the operational limits of commercial heat pumps currently available [16], storage temperatures up to 100 to 130 °C could be considered. Within this temperature range, sensible liquid heat storage is often applied in Rankine-based PTES as it is reliable, mature and cost-efficient. A two-tank configuration guarantees almost constant charge and discharge profiles [17]. It was thus selected instead

of a single tank solution, despite the cost of doubling the storage volume [18]. Water tanks were opted for as they are cheap, have low environmental impact, are suitable for the temperature range of interest and are commercially available for large capacities [5]. The hot tank temperature was chosen at 95 °C, while a cold tank temperature of 70 °C was assumed. This specific hot temperature was chosen to avoid pressurizing the tanks, which reduces the investment and maintenance costs [19]. The cold tank temperature of 70 °C was considered based on the trade-off between efficiency and storage density [20].

The basic heat pump topology in this work consists of four main components: an evaporator, a compressor, a condenser and an expansion valve. A topology with separate heat pump and ORC has been chosen over an alternative configuration using a single thermal machine as compressor (during charging) and expander (during discharging) or sharing heat exchangers between both operation modes. This was done because these *reversible* systems are currently less mature and limited to smaller system sizes, despite their lower investment cost [5]. In the literature, several advanced heat pump cycles have been proposed [16]. Although advanced cycles result in high efficiencies, the additional components increase the thermal capacitance of the system and are thus expected to slow down the system's dynamic response. Moreover, complex cycles require careful, simultaneous coordination of different control loops, which may further limit the obtainable ramping rates. Therefore, a basic system was assessed first. More complex topologies can be addressed in follow-up studies.

2.2. Nominal operating conditions and refrigerant selection

The boundary conditions above impose the temperature range of the heat pump. R1233zd(E) was chosen as working fluid as it shows good thermodynamic performance in the intended operating range, and has a low global warming potential and ozone depletion potential compared to refrigerants commonly used [21, 22]. Once the refrigerant was selected, the nominal operating conditions of the heat pump were determined using the steady-state cycle simulation tool CBSim developed by Laterre et al. [20]. Fluid property data were imported from REFPROP 10.0 [23]. Table 1 provides an overview of the boundary conditions and assumptions applied and the resulting nominal conditions. A more elaborate discussion on the assumptions can be found in [24].

Table 1. *Nominal operating conditions: modelling assumptions and results.*

Assumed parameter	Value	Unit	Output parameter	Value	Unit
$T_{water,source,in}$	60	°C	$p_{evaporator}$	1.83	bar
$T_{water,source,out}$	40	°C	$p_{condenser}$	10.10	bar
$T_{hot\ tank}$	95	°C	Pressure ratio	5.51	
$T_{cold\ tank}$	70	°C	$T_{evaporation}$	35.0	°C
p_{tank}	1	bar	$T_{condensation}$	98.5	°C
PP_{HX}	5	°C	$\dot{m}_{source}$	45.3	kg/s
Δp_{HX}	0	Pa	$\dot{m}_{WF}$	34.6	kg/s
$SH_{compressor,in}$	7.5	°C	$\dot{m}_{TES}$	50.35	kg/s
$\eta_{is,compressor}$	0.75	-	$\dot{Q}_{evaporator}$	3.79	MW
$P_{HP,net}$	1.5	MWe	$\dot{Q}_{condenser}$	5.29	MW
Refrigerant	R-1233zd(E)		COP	3.5	-
TES fluid	water				

2.3. Component selection and modelling

Components were selected based on the nominal conditions above and dynamically modelled. The dynamic model was programmed in the object-oriented language Modelica, using Dymola 2022 [25] and the TIL-library 3.14.0 [26]. The components of this library were used, and extended when necessary. Fluid properties were calculated using the REFPROP-database [23]. A detailed breakdown of the models and adaptations is provided in [24].

2.3.1. Heat exchangers

Plate heat exchangers (PHE) were selected for the evaporator and condenser because they are relatively cheap, very compact and have a modular design [18, 27]. Gasketed PHEs with capacities up to 30 MWth and volume flow rates up to 4500 m³/h are available [28]. The cross-sectional flow area and surface area in a PHE are interdependent, making precise matching of the thermal and hydrodynamic load difficult [29]. The rather

high volumetric flow rates make the heat exchanger pressure drop the dominant sizing constraint for the current application. Therefore, smaller plates and more parallel flow channels were selected to increase the cross-sectional area and thus reduce the pressure drop. Funke FP205 plates were chosen [28]. As the internal geometry is not published by the manufacturer, a reasonable assumption was made based on the literature. Typical corrugation depths of (industrial) heat exchangers range from 1.5 to 5.4 mm, resulting in identical plate spacing [29]. The inside geometry tested by Lee et al. [30] was used. It has a pattern amplitude of 0.97 mm, a pitch length of 7.5 mm and a chevron angle of 60 °. The pattern amplitude and pitch length were doubled to deal with the high volume flow rates, while the chevron angle of 60 ° was maintained. These updated dimensions still fall within the common range. The PHEs were modelled using the finite volume (FV) model available in the TIL-library [26], assuming countercurrent flow. FV-models have proven reliable for the dynamic simulation of evaporators and condensers [27]. Moreover, this PHE-model of the TIL-library was successfully used to simulate the dynamic behaviour of large-scale thermal cycles [31, 32]. On the refrigerant side, following heat transfer correlations were applied: Lee et al. [30] for evaporation, Zhang et al. [33] for condensation and Chisholm and Wanniarachchi [34] for single phase flow. Heat transfer at the water side was modelled by the Martin correlation [35]. Finally, refrigerant evaporation and condensation pressure drops were calculated by [30] and [33] respectively. [35] was used for all single phase pressure drops.

2.3.2. Compressor

A rotary screw or centrifugal compressor would be the most suitable compressor type taking the required flow rates and pressure ratio into account [36]. The operating conditions lie on the interface between volumetric and turbocompressors. Variable-speed twin-screw compressors maintain a high off-design efficiency in a wide range of part-load conditions, which makes them suitable for flexible operation [37]. Moreover, a recent market study illustrates that volumetric machines are often opted for in high temperature heat pumps with comparable capacity [22]. On the other hand, turbomachines have higher nominal efficiencies and their behaviour is scalable to higher capacities. Considering the focus on flexible operation in this work, a variable-speed twin-screw compressor was opted for. It is interesting to extend this methodology to turbocompressors in future work.

A performance-map based approach was followed to model the compressor due to the lack of detailed calibration data for more advanced semi-empirical models. Performance data of a suitable twin-screw compressor with variable internal volume ratio was retrieved from the manufacturers [38]. Isentropic and volumetric efficiency polynomials were than fitted to this data, as described in [32]. The off-design characteristics take the part-load compressor performance into account, but neglect the rotational inertia and thermal capacitance of the component. The rotational inertia is commonly neglected in dynamic modelling of Rankine-based thermal systems [27, 31]. This practice is followed in this paper. However, this assumption has been explicitly verified due to the interest in the electrical response [24]. This work focuses on power modulation during operation of the cycle and it is thus assumed that the system is warm. Given that the thermal capacitance of the compressor is small compared to the thermal capacitance of the heat exchangers, it was assumed negligible during power ramping. The influence of the compressor thermal capacitance on the system's startup behaviour should be assessed in future work.

2.3.2. Valve

The expansion valve is used to control the pressure levels in the heat pump cycle. Therefore, a valve with a controllable throughflow area is selected. In this work, no specific valve type is selected. Instead, common flow characteristics are assumed. The maximum opening is selected so that it never becomes limiting during operation. The expansion valve in the heat pump is modelled using the *OrrificeValve*-model from the TIL-library. It assumes that the internal volume of the valve is negligible and expansion is isenthalpic. The mass flow rate through the valve is related to the pressure drop across it using Saint-Venant and Wantzel correlation because of its applicability to compressible fluids.

2.3.3. Other components

A separator was added to the heat pump to extend the part-load operation range, as it helps buffering the varying refrigerant charge in the heat exchangers under different operating conditions. The separator splits the incoming refrigerant in a liquid and gas phase. It has been added at the high-pressure side, at the condenser outlet. As such, the separator imposes saturated liquid conditions at the valve inlet. At this position, the separator is useful for handling large refrigerant hold-up fluctuations [39]. It is modelled using the existing *Separator*-model of the TIL-library assuming and ideal separation characteristic.

The two-tank sensible storage system was not modelled in detail. Instead, it is represented by boundary models. This is a common approach to model two-tank storage in studies focusing on power modulation of PTES [32, 40]. The temperature at the condenser inlet was assumed constant at 70 °C, while the mass flow rate coming from the cold tank boundary could be controlled. Moreover, the water pressure at the condenser

outlet was assumed constant and imposed with another boundary. The water temperature at the condenser outlet is thus not imposed, but follows directly from the heat pump operation.

2.4. Controller design

The heat pump should respond quickly to a desired power uptake, while maintaining the set storage temperatures and maximizing operational efficiency. Moreover, a low part-load ratio is desirable to maximize the capacity available for flexibility services.

The control strategy implemented to realize this is visualized in Figure 2. It uses three PI-controllers steering the compressor rotational speed (blue), valve throughflow area (red) and water mass flow rate in the condenser (green).

Variable-speed control of the compressor is an effective way to modulate the electrical power uptake [31, 32]. Therefore, the compressor PI-controller compares the desired power uptake ($Pdrive,set$) with the effective one ($Pdrive,m$) and changes the rotational speed accordingly. The minimum and maximum saturation values of the compressor speed were set as 25 Hz and 60 Hz, corresponding to the minimum and maximum indicated by the manufacturer [38].

As the operating point is determined by the intersection of the compressor and valve characteristic, a change in compressor speed influences the pressure levels in the cycle. Therefore, a second PI-controller for the valve is used to control its effective throughflow area to maintain a suitable superheat level at the compressor inlet. A setpoint of 7.5 °C is implemented (instead of lower values of 3 and 5 °C often assumed in thermodynamic optimizations) to increase the part-load range and avoid condensation during power ramping.

Finally, the water mass flow rate in the condenser was adapted by the TES PI-controller to maintain a hot storage temperature of 95 °C by comparing this setpoint to the measured temperature at the condenser outlet.

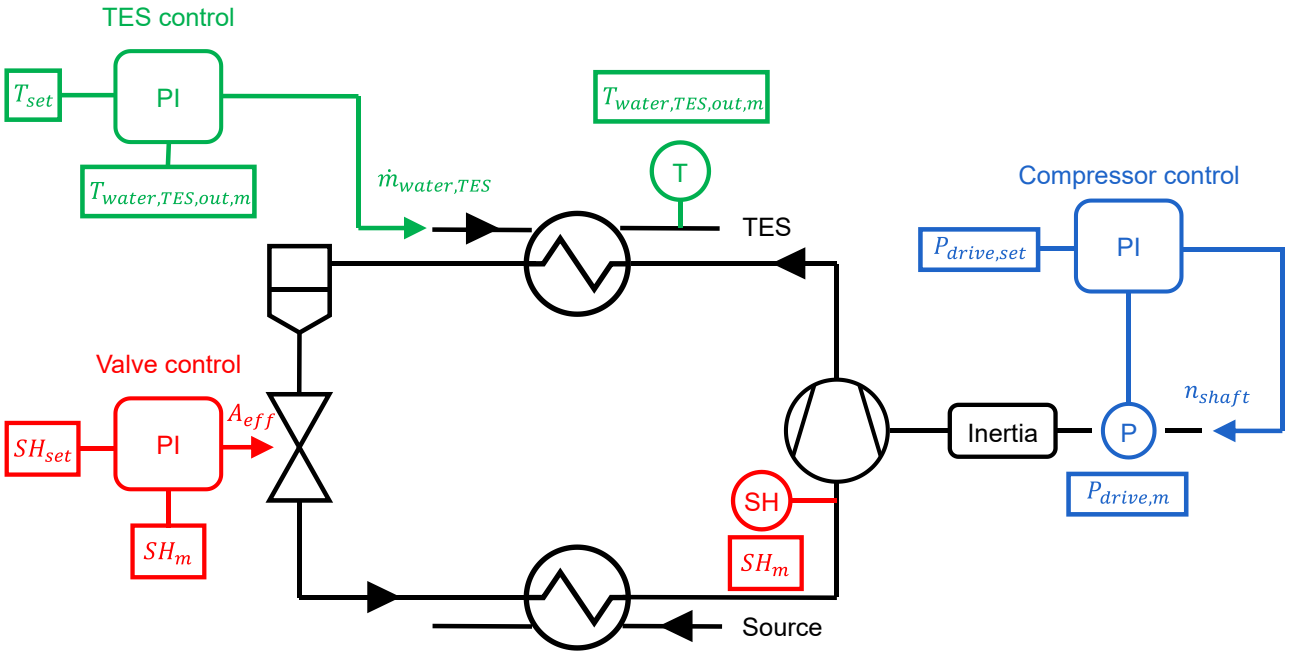

Figure. 2. *Schematic representation of the heat pump control strategy.*

All PI-constants were determined based on step-response analysis using an in-house tuning tool based on the Mathworks System Identification Toolbox. The PI-control settings are summarized in Table 2.

Table 2. *Heat pump PI-control settings.*

Controller	k [−]	T_i [s]	Min sat value	Max sat value
Compressor	3.0927e-05	0.3681	25 [Hz]	60 [Hz]
Valve	3.4773e-05	1.2029	$0.2 \cdot A_{nom}$[m²]	$2 \cdot A_{nom}$[m²]

Water $\dot{m}$	1.4515	4.5859	$0.2 \cdot \dot{m}_{nom}$ [kg/s]	$2 \cdot \dot{m}_{nom}$ [kg/s]

2.5. Solar PV load-following test

When integrated locally, the heat pump have a sufficiently fast response to follow the instantaneous fluctuations of solar PV production. Testing this thus requires high resolution (1 to 5 s) representative solar PV data or output predictions, which is hard to find. Most open-source models predict solar PV production based on 10 min or hourly samples.

The heat transfer and alternative energy system group at NIST recognized this issue and made available 1 second and 1 minute data of their photovoltaic testbeds [41]. In this study, online power measurements of a 271 kWp DC ground-mounted PV array in Gaithersburg (MD) USA (39.1319 °, -77.2141 °) were used. Instantaneous data was collected with a sampling time of 1 s for the years 2016-2018. The 2018 data was used in this work. Note that the 271 kWp peak capacity is smaller than the 1.5 MW charge power of the heat pump modelled. Therefore, the data will be scaled to a peak capacity of 1.5 MW (see Section 2.5.2.). As demonstrated by Marcos et al. [12] the PV power fluctuations are not only influenced by the intermittence of cloudiness but also by the plant size. Larger PV plant sizes tend to smooth out power fluctuations, which is especially noticeable at short sampling times. Scaling this data to higher system sizes is thus a conservative approach to validate the system dynamics.

To limit the simulation time, the power gradients were calculated from the annual data and the day with the highest power gradient was further analyzed. For this dataset, the highest power gradients occurred on June 4th. The corresponding power profile is shown in Figure 3 (a). The solar power profile shows the expected average evolution. Before sunrise and after sundown the production equals zero. The solar production peaks around noon corresponding to the periods with maximum solar irradiation. Despite this expected average trend, the power fluctuates significantly around this average, illustrating the importance of checking the dynamic compatibility.

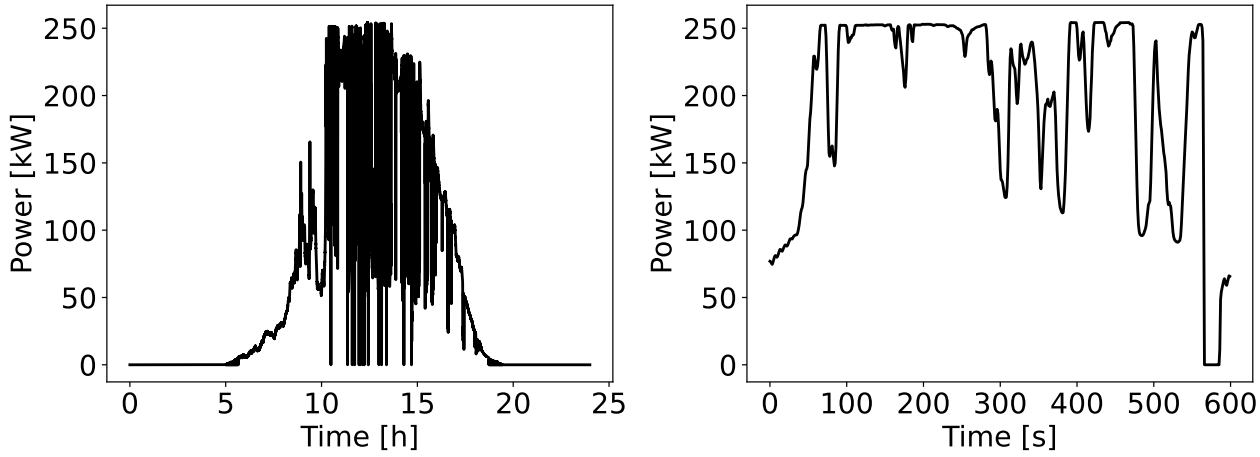

Figure. 3. *Representative solar PV production of a 271 kWp installation. a) shows the daily profile and b) the selected 10 min test sample.*

The data has also some zero values during the day, which are typically caused by faulty signals or curtailment due to excessively high grid voltage. The maximum gradient found is caused by one of these sudden zero values. After the profile scaling discussed in Section 2.5.2., a 10 min interval around this maximum reduces to a constant power with three peaks. Therefore, a more representative 10 min test interval close to this maximum was selected. The highest gradient in this test sample equals 98 % of the overall maximum, while it better represents the typical subsequent power fluctuations. This test sample is shown in Figure 3 (b).

Note that this analysis aims to provide primary insights in the technical potential of large-scale heat pumps only. A more thorough assessment based on high resolution data from multiple locations and PV plant sizes and selection of statistically relevant scenarios is recommended to formulate a decisive general conclusion.

2.5.1. Limitations of PTES and the current modelling approach

The profiles above illustrate that solar PV production regularly has periods with low or even no power generation. The zero production before sunrise and after sundown is expected and predictable. Therefore, the heat pump startup and shutdown can be planned in this case. However, in previous analysis the part-load range of the heat pump in nominal operation has been determined as around 50 % of its nominal capacity [24]. If the VRE fluctuations exceed this range, perfect uptake of the power profile would thus require regular startup and shutdown of the heat pump during the day as well. Depending on the envisaged operating scenario, even switching between charge and discharge mode might be required. As an example, such switching is needed when the storage is used to smooth the VRE power ramping rate at the grid connection point or when provision of constant grid power at an average value would be envisaged, as illustrated for Li-ion batteries in [42].

Switching between charge and discharge mode is typically assumed immediate in techno-economic studies, which is reasonable if the startup and shutdown time are short compared to the 15 min or 1 h timestep. However, the realistic power profiles highlight that more frequent and fast startup might be required in some load-shifting scenarios. Moreover, these studies often assume the full power capacity can be used and thus neglect the limited part-load range of real heat pumps and ORCs. Careful sizing of the VRE and cycle capacity and operational planning should thus be considered. These considerations illustrate the need for a detailed look at the startup and shutdown behaviour of PTES and further inclusion of technical limitations in techno-economic studies.

2.5.2. Scaling procedure of the solar PV profile to heat pump operating range

The control structure and modelling approach presented in this paper focus on the heat pump power modulation while in use. Therefore, it can be used only to verify the dynamics during nominal operation. The heat pump part-load range is limited between 750 kW and 1.5 MW. Starting from the measured data above, dynamic test profiles are constructed as follows:

- The collected PV data contains values below zero due to measurement errors for almost zero production. Therefore, these negative values are replaced with zero values first.
- The original power profile is normalized with the peak capacity installed. The normalized power thus remains between zero and one.
- The normalized profile is scaled to the nominal heat pump capacity by multiplying all values with 1.5 MW.
- The scaled profile might contain fluctuations exceeding the modulation range of the heat pump. Therefore, all values below 750 kW are replaced with this value.
- Finally, a sufficiently long initial settling period is added to the profile to ensure the results are independent of the model initialization. This settling period is added at the initial power of the VRE test sample to ensure steady-state at the test start.

A schematic of this procedure and the resulting test profiles is provided in Figure 4. Practically, the resulting profile corresponds with a situation where the VRE production is complemented by grid electricity to maintain a minimum base load for the heat pump. Passing clouds, sudden drops in wind, and curtailment due to excessive grid voltage are local phenomena. It is thus reasonable to assume that sufficient VRE generation is available globally when the heat pump is used to charge, which corresponds to low grid electricity prices. This assumption allows to verify whether the heat pump dynamics can satisfy the fast response during nominal operation. The model could be extended to include startup and shutdown behaviour to evaluate these dynamics in alternative operating scenarios.

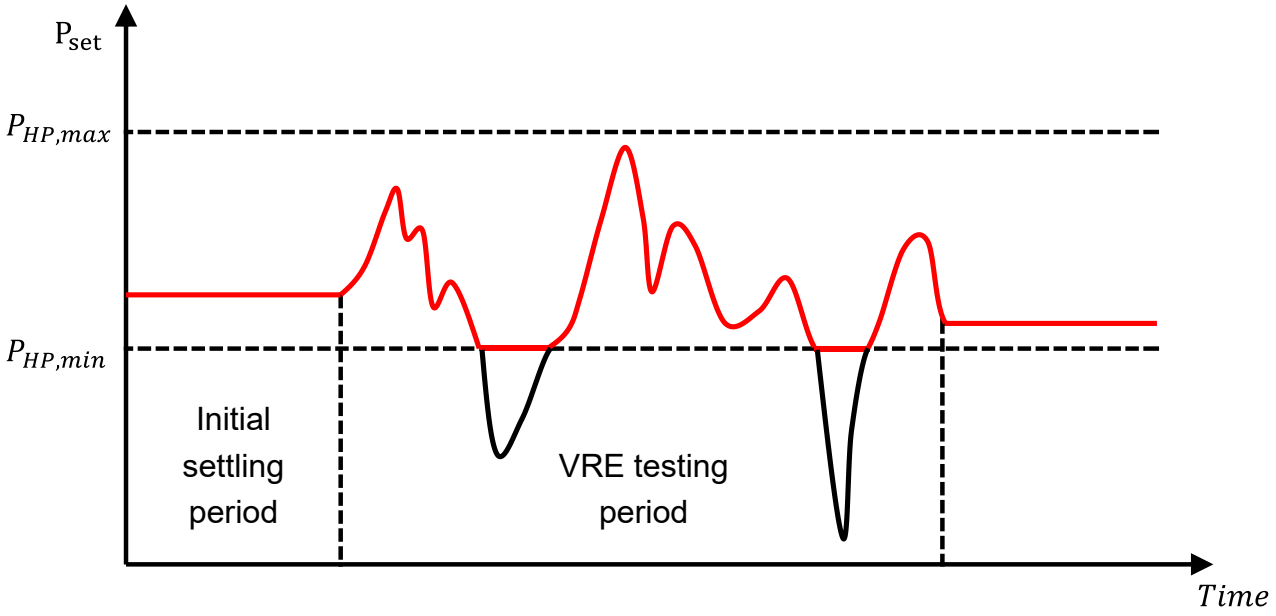

Figure. 4. *Visualization of the VRE test profile.*

3. Results

The solar PV measurement data for the load-following test is shown in Figure 3 (b). The scaled power profile fitting the heat pump operating range and the system power response are shown in Figure 5.

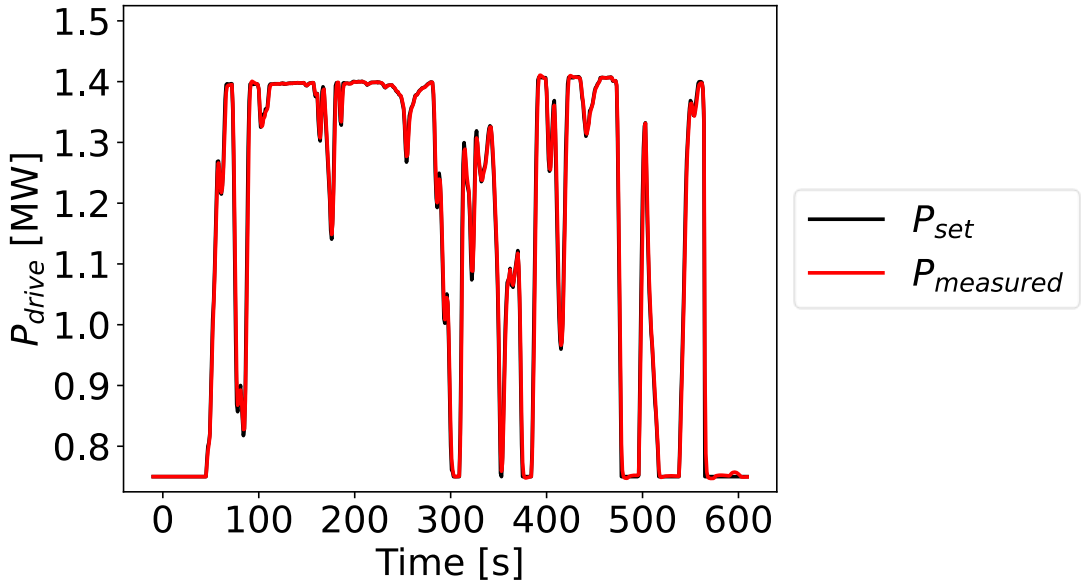

Figure. 5. *Power response of a 1.5 MW heat pump during a load-following test for solar PV.*

The solar PV fluctuations exceed the modulation range and grid electricity is thus used to maintain a base load during 140 s. Overall, the heat pump dynamics match well with the solar PV generation as the black power setpoint is almost fully covered by the red simulated response. The maximum relative power deviation equals 19.3 % and occurs after 565 s. This deviation corresponds with the maximum power gradient of 318 kW/s, caused by a sudden drop to base load. At this rate, it would only take 2.36 s to ramp between 1.5 MW and 750 kW. Direct load-following of solar PV thus requires rather high ramping rates. The observed deviations can be placed into context by the grid balancing requirements issued by the TSO. The Belgian TSO allows a relative power deviation margin of 7.5 % of the desired capacity during the load-following test for secondary frequency reserve services, which might be exceeded for maximally 30 timesteps of 4 s during the 90 min test [43]. In this load-following test, the maximum deviation exceeds this margin but this happens only during one 1 s timestep. The overall match is confirmed by the aggregated absolute error between the setpoint and actual HP power uptake of 1.263 kWh, which corresponds to 0.66 % of the planned power uptake.

Interestingly, the instantaneous HP power uptake is sometimes higher and sometimes lower than the setpoint. It slightly lags the bidirectional fluctuations, which means the error averages out over the test interval. In fact, the net aggregated error over the full test interval equals only -0.0172 kWh or -0.009 % of the requested energy uptake. From an energetic point of view, the actual heat pump power uptake thus marginally exceeds the desired one over the 10 min test interval, indicating the dynamic compatibility within the heat pump modulation range.

Suitable TES temperatures should be maintained during the test. This temperature response is visualized in Figure 6. The maximum absolute TES delivery temperature deviation equals 4.38 °C. Although this exceeds the expected accuracy of platinum RTDs (0.1 to 1 °C), it just remains within the typical measurement accuracy of industrial thermocouples (0.5 to 5 °C) [44]. It can be seen the TES delivery temperature fluctuates around its setpoint due to the fast fluctuating power. The temperature response lags the power response and quickly returns to the setpoint when the power uptake stabilizes. The deviations average out over the test interval and the mean delivery temperature equals 94.99 °C. These deviations are thus certainly acceptable.

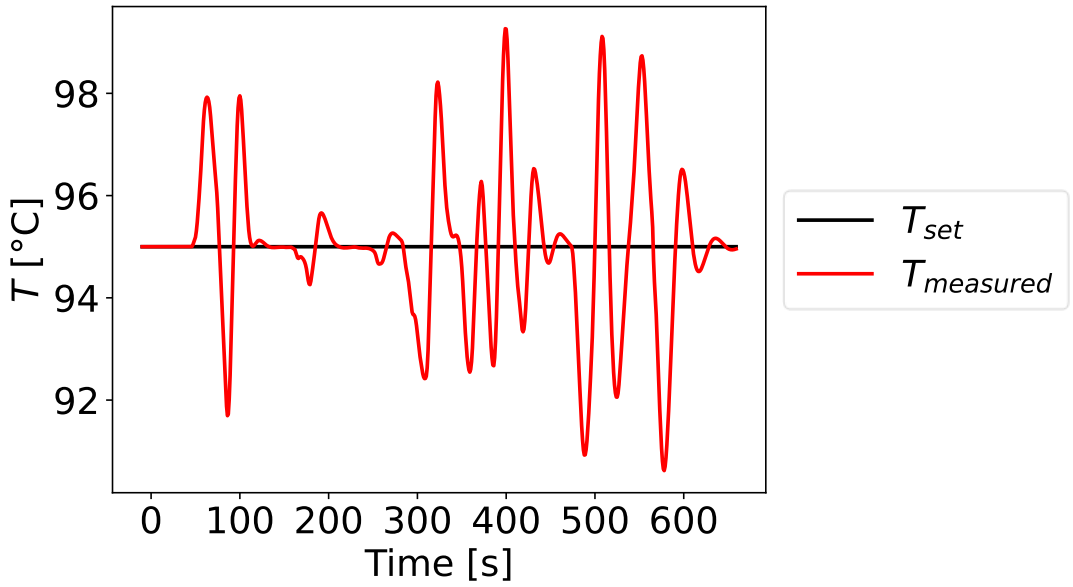

Figure 6. *TES delivery temperature response of a 1.5 MW heat pump during a load-following test for solar PV.*

To conclude this feasibility analysis, the operating conditions of the different components were briefly verified. The main challenge observed was maintaining superheated conditions at the compressor inlet. During the test, the minimum superheat at the compressor inlet and outlet became 1.34 and 7.70 °C during the sudden drop to base load at the end of the test. Except for this one instance the superheating at the compressor inlet and outlet remained above 4 °C. While this is acceptable for the volumetric machine used, it thus illustrates the importance of an adequate control strategy or additional countermeasures to avoid two-phase conditions during fast ramping. According to literature [31, 45], preheating the suction line or implementation of an internal heat exchanger could further mitigate the condensation risk.

4. Conclusion

This paper verified the technical feasibility of load-following solar PV production with variable-speed vapour compression heat pumps. The solar PV profile is based on measured data of a 271 kWp installation which is scaled to the 1.5 MW system in this study. As power fluctuations caused by clouds are dampened more with increasing PV plant size, the scaled fluctuations are thus higher than would be expected for an actual installation with increased peak capacity. This is thus a conservative estimation. The results indicate the heat pump dynamics are suitable for direct load-following of solar PV. Although the maximum relative power deviation for solar PV equals 19.3 %, it only happens with the maximum power gradient caused by a sudden drop of the PV production to zero, and thus of the heat pump setpoint to base load. The relative deviation remains below 7.5 % for the remainder of the test. Moreover, the aggregated absolute error between the setpoint and actual heat pump power uptake accounts for only 0.66 % of the desired uptake. The TES delivery temperature fluctuates around its setpoint and quickly returns to this point in stable power periods. A maximum temperature deviation and average TES-delivery temperature of 4.38 °C and 94.99 °C were determined, respectively. The PTES dynamics are thus suitable for direct load-following of variable solar PV during

charging. However, a more thorough assessment based on high resolution data from multiple locations and plant sizes and selection of statistically relevant scenarios is recommended to formulate a decisive general conclusion. Moreover, inclusion of startup and shutdown behaviour would allow to evaluate these dynamics in alternative operating scenarios. Finally, an extension of this analysis to wind generation would be valuable to cover both main VRE electricity sources.

Nomenclature

A	area, m²
COP	coefficient of performance, -
$\dot{m}$	mass flow rate, kg/s
p	pressure, Pa
PP	pinch point, K
$\dot{Q}$	heat transfer rate, W
SH	superheat, K
T	temperature, K

Greek symbols

Δ	difference
η	efficiency

Subscripts and superscripts

eff	effective
HP	heat pump
HX	heat exchanger
in	inlet
is	isentropic
m	measured, sensor value
max	maximum
min	minimum
nom	nominal
out	outlet
set	setpoint
TES	thermal energy storage system
WF	working fluid

References

[1] Enerdata. World Energy & Climate Statistics – Yearbook 2025 – Available at: <https://yearbook.enerdata.net/renewables/renewable-in-electricity-production-share.html> [accessed 16.02.2026].

[2] Rosslowe C., Petrovich B., European Electricity Review 2025. EMBER; 2025 Jan.

[3] Graham E., Fulghum N., Altieri K., Global Electricity Review 2025. EMBER; 2025 April.

[4] Argyrou M.C., Christodoulides P., Kalogirou, S.A., Energy storage for electricity generation and related processes: Technologies appraisal and grid scale applications. Renewable and Sustainable Energy Reviews 2018;94:804-21.

[5] Dumont O., Frate G.F., Pillai A., Lecompte S., De Paepe M., Lemort V., Carnot battery technology: A state-of-the-art review. Journal of Energy Storage 2020;34:101756.

[6] McTigue J.D., Farres-Antunez P., Sundarnath J.K., Markides C.N., White A.J., Techno-economic analysis of recuperated Joule-Brayton pumped thermal energy storage. Energy Conversion and Management 2022;252:115016.

[7] Vecchi A., Knobloch K., Liang T., Kildahl H., Sciacovelli A., Engelbrecht K., Li Y., Ding Y., Carnot Battery development: A review on system performance, applications and commercial state-of-the-art. Journal of Energy Storage 2022;55:105782.

[8] Tassenoy R., Couvreur K., Beyne W., De Paepe M., Lecompte S., Techno-economic assessment of Carnot batteries for load-shifting of solar PV production of an office building. Renewable Energy 2022;199:1133-44.

[9] Frate G.F., Ferrari L., Sdringola P., Desideri U., Sciacovelli A., Thermally integrated pumped thermal energy storage for multi-energy districts: Integrated modelling, assessment and comparison with batteries. Journal of Energy Storage 2023;61: 106734.

[10] Ghilardi A., Frate G.F., Kyprianidis K., Tucci M., Ferrari L., Brayton pumped thermal energy storage: Optimal dispatchment in multi-energy districts. Energy Conversion and Management 2024;314:118650.

[11] Laterre A., Frate G.F., Lemort V., Contino F., Carnot batteries for integrated heat and power management in residential applications: A techno-economic analysis. Energy Conversion and Management 2025;325:119207.

[12] Marcos J., Marroyo L., Lorenzo E., Alvira D., Izco E., Power output fluctuations in large scale pv plants: One year observations with one second resolution and a derived analytic model. Progress in Photovoltaics: Research and Applications 2011;19:2018-27.

[13] Lave M., Kleissl J., Arias-Castro E., High-frequency irradiance fluctuations and geographic smoothing. Solar Energy 2012;86(8):2190-99.

[14] Frate G.F., Antonelli M., Desideri U., A novel Pumped Thermal Electricity Storage (PTES) system with thermal integration. Applied Thermal Engineering 2017;121:1051-58.

[15] Marina A., Spoelstra S., Zondag H.A., Wemmers A.K., An estimation of the European industrial heat pump market potential. Renewable and Sustainable Energy Reviews 2021;139:110545.

[16] Arpagaus C., Bless F., Uhlmann M., Schiffmann J., Bertsch S.S., High temperature heat pumps: Market overview, state of the art, research status, refrigerants, and application potentials. Energy 2018;152:985-1010.

[17] Sciacovelli A., Vecchi A., Ding Y., Liquid air energy storage (LAES) with packed bed cold thermal storage – From component to system level performance through dynamic modelling. Applied Energy 2017;190:84-98.

[18] Frate G.F., Ferrari L., Desideri U., Multi-Criteria Economic Analysis of a Pumped Thermal Electricity Storage (PTES) With Thermal Integration. Frontiers in Energy Research 2020;8:53.

[19] Dahash A., Ochs F., Janetti M.B., Streicher W., Advances in seasonal thermal energy storage for solar district heating applications: A critical review on large-scale hot-water tank and pit thermal energy storage systems. Applied Energy 2019;239:296-315.

[20] Laterre A., Dumont O., Lemort V., Contino F., Extended mapping and systematic optimisation of the Carnot battery trilemma for sub-critical cycles with thermal integration. Energy 2024;304:132006.

[21] Frate G.F., Ferrari L., Desideri U., Analysis of suitability ranges of high temperature heat pump working fluids. Applied Thermal Engineering 2019;150:628-40.

[22] Zühlsdorf B., Poulsen J.L., Dusek S., Wilk V., Krämer J., Rieberer R., Verdnik M., Demeester T., Vieren E., Magni C., Abedini H., Leroy C. Yang L., Andersen M.P., Elmegaard B., Turunen-Saaresti T., Uusitalo A., De Carlan F., Gachot C., Schlosser F., Klöppel S., Khass O.A., Schaffrath R., Wittstadt U., Henninger S., Teles de Oliveira H., Kaida T., Ramirez M., Lycklama a Nijeholt J., Schlemminger C., Moen O.M., Lee G., Arpagaus C., Annex 58 High-Temperature Heat Pumps Task 1 – Technologies, Heat Pump Centre c/o RISE, 2023 August. Technical Report No.: HPT-AN58-2.

[23] Lemmon E.W., Bell I.H., Huber M.L., McLinden M.O., NIST Standard Reference Database 23: Reference Fluid Thermodynamic and Transport Properties - REFPROP, Version 10.0. National Institute of Standards and Technology; 2018.

[24] Tassenoy R., Dynamic Behaviour of Large-Scale Vapour Compression Heat Pumps in Carnot Batteries for Grid Services [dissertation]. Ghent, Belgium: Ghent University, 2026.

[25] Dassault Systemes, Dymola 2022, 2022.

[26] TLK-Thermo GmbH, TIL Library – Version 3.14.0, 2023.

[27] Imran M., Pili R., Usman M., Haglind F., Dynamic modeling and control strategies of organic Rankine cycle systems: Methods and challenges. Applied Energy 2020;276:115537.

[28] Funke, Plate Heat Exchangers: series FP, FPDW, 2023.

[29] Wang L, Sundén B., Manglik R.M., Plate Heat Exchangers - Design, Applications and Performance. Southamption, UK: WIT Press; 2007.

[30] Lee D., Kim D., Park S., Lim J., Kim Y., Evaporation heat transfer coefficient and pressure drop of R-1233zd(E) in a brazed plate heat exchanger. Applied Thermal Engineering 2018;130:1147-55.

[31] Meesenburg W., Markussen W.B., Ommen T., Elmegaard B., Optimizing control of two-stage ammonia heat pump for fast regulation of power uptake. Applied Energy 2020;271:115126.

[32] Tassenoy R., Laterre A., Lemort V., Contino F., De Paepe M., Lecompte S., Assessing the influence of compressor inertia on the dynamic performance of large-scale vapor compression heat pumps for Carnot batteries. Journal of Energy Storage 2024;101:113948.

[33] Zhang J., Elmegaard B., Haglind F., Condensation heat transfer and pressure drop correlations in plate heat exchangers for heat pump and organic Rankine cycle systems. Applied Thermal Engineering 2021;183:116231.

[34] García-Cascales J.R., Vera-García F., Corberán-Salvador J.M., Gonzálvez-Marciá J., Assessment of boiling and condensation heat transfer correlations in the modelling of plate heat exchangers. International Journal of Refrigeration 2007;30(6):1029-41.

[35] Martin H., N6 Pressure Drop and Heat Transfer in Plate Heat Exchangers. In: VDI Heat Atlas. Berlin, Germany: Springer. 2010. p. 1515-20.

[36] Hoopes K., Allison T.C., Kurz R., Oil and Gas Compressor Basics. In: Brun K., Kurz R., editors. Compression Machinery for Oil and Gas. Houston, USA: Gulf Professional Publishing. 2019. p. 3-11.

[37] Brasz J.J., Comparison of Part-Load Efficiency Characteristics of Screw and Centrifugal Compressors. In: Proceedings of the International Compressor Engineering Conference; 2006; West Lafayette, USA. Purdue e-Pubs: 1827.

[38] GEA Heating & Refrigeration Technologies, RTSelect software, 2024.

[39] SWEP. Refrigeration handbook – chapter 7: condensers – Available at: <https://www.swep.fr/refrigerant-handbook/7.-condensers/asd4/> [accessed 17.06.2025]

[40] Frate G.F., Pettinari M., Di Pino Incognito E., Costanzi R., Ferrari L., Dynamic modelling of a Brayton PTES system. In: ASME Turbo Expo 2022 Turbomachinery Technical Conference and Exposition (GT2022); 2022 Jun 13-17; Rotterdam, The Netherlands. ASME: 1-14.

[41] Boyd M., Performance Data from the NIST Photovoltaic Arrays and Weather Station. J Res Natl Inst Stand Technol 2017;122:1-4.

[42] Marcos J., Sorkël O., Marroyo L., Garcia M., Lorenzo E. Storage requirements for PV power ramp-rate control. Solar Energy 2014;99:28-35.

[43] Elia, Balancing Service Providers Contract for the automatic Frequency Restoration Reserve (aFRR) Service "BSP Contract aFRR". 2024.

[44] RS Pro, RS Pro - Platinum Resistance Thermometer (PRT) Selection Guide. 2024

[45] Meesenburg W., Kofler R., Ommen T., Markussen W.B., Elmegaard B., Design considerations for dynamically operated large-scale ammonia heat pumps. In: Proceedings of the 25th IRR International Congress of Refrigeration; 2019; Paris, France. International Institute of Refrigeration: 2591-98.